Proceedings of the 2005 IEEE
International Conference on Robotics and Automation
Barcelona, Spain, April 2005

Fast Dense Panoramic Stereovision

Jose-Joel Gonzalez-Barbosa*
Universidad de Guanajuato –FIMEE
Tampico 912
36730 Salamanca, Gto. M´exico
barbosa@salamanca.ugto.mx

Simon Lacroix
LAAS-CNRS
7, Av. du Colonel Roche
31077 Toulouse Cedex 4 France
Simon.Lacroix@laas.fr

***Abstract*-- The particular geometry of panoramic cameras defines complex epipolar lines equations. In this paper, we present a way to warp images from a panoramic stereovision bench, so that the epipolar lines become parallel straight lines, thus allowing the use of an optimized fast pixel correlation based stereovision algorithm. The paper first introduces the geometric characterization of panoramic camera composed of parabolic and spherical mirrors, that computes both the intrinsic parameters of the system (mirror surfaces and intrinsic camera parameters) and the errors alignment between the mirrors. Then, it presents the warping equations that allow to generate rectified images. Calibration and stereovision results are presented.**

***Index Terms*- Panoramic images, calibration, epipolar lines, stereovision**

II. INTRODUCTION

For the purpose of path planning and obstacle avoidance, a detailed analysis is not necessarily required, and high speed and rough understanding of the environment around the robot can be sufficient. One effective way to enhance the field of view with high speed of acquisition is to use of catadioptric panoramic cameras, i.e. convex mirrors in conjunction with lenses.

Omnidirectional cameras with a single center of projection allow the generation of images projected on any given surface, such as a pure perspective images or panoramic images. Indeed, with the single viewpoint property, every pixel in the sensed image measures the light passing through the viewpoint in one particular direction: we will show that this property also allows to rectify panoramic image pairs, and therefore to apply an optimized pixel correlation based algorithm.

Various contributions on panoramic stereovision can be found in the literature (e.g. [9, 20, 1, 3, 12, 17, 19, 13]), but most of them consider that the catadioptric system is perfectly aligned, which is seldom the case for actual cameras. Stereo has been obtained in panoramic images with perfectly aligned cameras positioned one above the other [9, 20]. The main advantage of this alignment is that the epipolar curves are reduced to radial lines. But in several applications this alignment can't be used, in the case of environment modeling with several panoramic cameras [16, 4, 10] for instance.

In this paper, we present an algorithm to perform fast stereovision with a pair of panoramic cameras positioned in any configuration. For that purpose, a precise calibration of the cameras is required: the following section presents a full characterization of a panoramic camera composed of a parabolic and a spherical mirrors, introducing the system misalignment errors. Section III describes the calibration procedure to estimate all the parameters of the camera geometric model, and section IV presents the epipolar geometry of a panoramic stereovision system, and a way to rectify the panoramic images. Results are presented throughout the paper.

II. CHARACTERIZATION OF THE OMNIDIRECTIONAL VISION SENSOR

A. Related work

Several catadioptric camera calibration methods have been proposed in the literature. In [5], the authors use a catadioptric camera with a conic mirror. They present a sensor characterization and proposes a method to calibrate it using different calibration pattern. The calibration method in [15] uses the bounding circle of the omnidirectional image. The parabolic parameter and the mirror axis are directly computed using the radius and circle center. The method proposed in [11] uses the circle-based calibration method to initialize a minimization function. A self-calibration method using point features tracked across an omnidirectional image sequence is proposed. In [8], the authors introduce the catadioptric line projection for catadioptric calibration. The projection of two sets of parallel lines is sufficient to compute the parabolic mirror parameter and its optical projection axis in the image. The calibration method proposed in [6] assumes that the mirror surface parameters are known, and estimate the intrinsic parameters of the camera with respect to the mirror, using the two circles appearing in the image corresponding to a known section of the mirror. All the previous models suppose that the alignment between the camera and the mirror is perfect: the authors in [18] present a full model of the imaging process that includes the translation and rotation between the camera and the mirror that uses tracked points across a sequence. In [13], a theory that describes the image formation is proposed, with an auto-calibration of central omnidirectional cameras.

B. Perfectly aligned configuration

Figure 1 presents the geometry of image formation for a catadioptric camera built with parabolic and spherical mirrors, and the various associated frames. For the characterization of this system, we use the following notations: 3D points are represented by bold upper case letter, while 3D point projections on any surface are represented by bold lower case letters. The entities with subscript w refer to the world coordinate system W and entities with subscript c, p, s refer to the camera, parabolic and spherical coordinate systems C, P, S respectively.

In Figure 1, the parabolic and spherical mirrors axes are superposed, and the conventional camera is placed on the projection center of the spherical mirror: the rays that intersect the conventional camera lens are parallel to the

*Jose-Joel Gonzalez-Barbosa is partially supported by the Project No PROMEP/103.5/04/1335

spherical and parabolic optical axis, and each perceived ray virtually intersects on P. The expression of the parabolic mirror surface is by the Equation (1) ([14]).

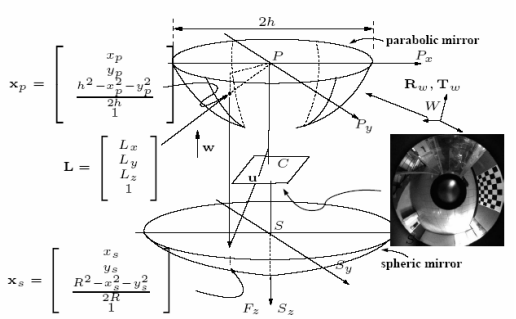

Fig. 1 An ideal catadioptric camera with a parabolic and spheroidal mirrors; it is assembled so that the optical axis of the conventional camera is aligned with the mirrors symmetry axis. The values u, x_p, x_s are homogeneous vectors, corresponding to image points, points on the parabolic and on the spherical surface respectively.

$$z = \frac{h^2 - (x^2 + y^2)}{2h} = \frac{h^2 - r^2}{2h} \qquad (1)$$

where h is the mirror parameter. The point $\mathbf{L}_w$ is transformed to the point $\mathbf{L} = [L_x, L_y, L_z]^T$ ($\mathbf{L} = R_w \mathbf{T}_w - \mathbf{T}_w$, see Figure 1) and projected by a central projection onto the surface of the mirror ($\mathbf{x}$) according to:

$$\mathbf{x}_p = \begin{bmatrix} x_p \\ y_p \\ 1 \end{bmatrix} = \begin{bmatrix} \frac{hL_x}{\sqrt{L_x^2 + L_y^2 + L_z^2} + L_z} \\ \frac{hL_y}{\sqrt{L_x^2 + L_y^2 + L_z^2} + L_z} \\ 1 \end{bmatrix} = \begin{bmatrix} \frac{hL_x}{Z'} \\ \frac{hL_y}{Z'} \\ 1 \end{bmatrix} \qquad (2)$$

where $Z' = |\mathbf{L}| + L_z$. After the projection on the parabolic surface, the ray intersects the spherical surface. The spherical mirror section is very small as compared to the spherical radius R: we can approximate the spherical surface using only the first term of the follow equation:

$$g(x,y) = \frac{R}{2} - \frac{x^2 + y^2}{2R} + \frac{1}{2}\frac{x^4 + y^4}{2^2 2! R^3} + \ldots \approx \frac{R^2 - x^2 - y^2}{2R}$$

In Figure 1, the camera lens is positioned in the focal point of the spherical mirror. Then the image plane is intersected by the parallel ray of optical axis of the spherical and parabolic mirror. This assumption allows us to have an orthographic projection in the parabolic mirror, and only one projection center in the parabolic surface. The points of the spherical mirror $\mathbf{x}_s$ are defined as a function of the points on the parabolic mirror by:

$$\mathbf{x}_s = \begin{bmatrix} x_p & y_p & \frac{R^2 - x_p^2 - y_p^2}{2R} & 1 \end{bmatrix}^T \qquad (3)$$

where x_p and y_p are given in Equation 2. Using the following equation, we obtain the perspective projection of x_s in the plane image defined in pixels.

$$\mathbf{u} = [su \quad sv \quad s]^T = I_C \mathbf{M}[R_{sc}, \mathbf{T}_{sc}]\mathbf{x}_s \qquad (4)$$

where I_C is the intrinsic matrix of the conventional camera [7], and $\mathbf{M}[R_{sc}, T_{sc}]$ is the translation and rotation homogeneous matrix between the spherical mirror S and the camera frame C.

In the ideal case the matrix $\mathbf{M}[R_{sc}, T_{sc}]$ is the identity matrix. Then, an ideal omnidirectional camera with parabolic and spherical mirror is characterized by:

$$u = \frac{-\alpha_u x_p (2R)}{R^2 - (x_p^2 + y_p^2)} + u_0 \qquad (5)$$
$$v = \frac{\alpha_v y_p (2R)}{R^2 - (x_p^2 + y_p^2)} + v_0$$

where (x_p, y_p) is given in Equation 2.

C. *Error alignment considerations*

The characterization defined by Equation 5 doesn't take into account the possible misalignments that come from the system assembly. Figure 2 shows a system with alignment errors: in this configuration, the rays captured by the conventional camera are parallel to optical axis of the spherical mirror, but not parallel to the optical axis of the parabolic mirror. Figure 3 shows the virtual reflection rays of the parabolic mirror in a system with a rotation angle of 5^o between the parabolic and spherical mirror: the lines inside of the surface are an extension of incident rays. For these lines, there is not only one intersection point, they are tangents to a caustic surface. If the rotation angle between the mirrors is small, the caustic surface can be approximated to a point $P' = [p'_x \quad p'_y \quad p'_z]$ that minimizes the projection error.

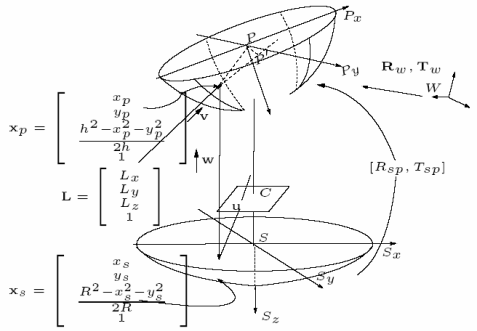

Fig. 2: A real panoramic camera using spherical and parabolic mirror.

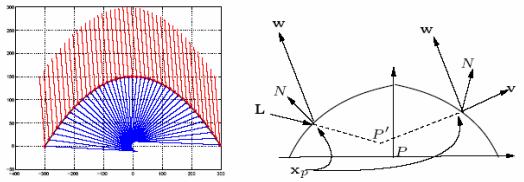

Figure 3: Reection of a parabolic mirror (outside of the surface) and incidents rays (inside of the surface). If the parabolic and spherical mirror are not aligned the incident rays are tangent to a caustic surface. On right, the caustic surface is approximated by the point P'.

Let $\mathbf{M}[R_{sp}, T_{sp}]$ the transformation matrix between the spherical mirror frame S and the parabolic mirror frame P, where R_{sp} and T_{sp} is the rotation and translation. The projection of incident rays in parabolic are parallel to $S_x(\mathbf{w})$, in the frame P. The direction w (see Figure 2) is given by:

$$w = \begin{bmatrix} R_{sp} & 0 \\ 0 & 1 \end{bmatrix} [0 \quad 0 \quad -1 \quad 1]^T$$

where $R_{sp} = \begin{bmatrix} 1 & 0 & 0 \\ 0 & \cos\theta_{sp}^x & -\sin\theta_{sp}^x \\ 0 & \sin\theta_{sp}^x & \cos\theta_{sp}^x \end{bmatrix} \begin{bmatrix} \cos\theta_{sp}^y & 0 & \sin\theta_{sp}^y \\ 0 & 1 & 0 \\ -\sin\theta_{sp}^y & 0 & \cos\theta_{sp}^y \end{bmatrix}$

Considering that the point P' is the intersection point of the incidents rays, the 3D point $\mathbf{L}$ is projected to parabolic surface (see Figure 3) according to:

$$P' - \mathbf{L} - \lambda(\mathbf{x}_p - \mathbf{L}) = \mathbf{0}$$

There are two possible solutions, the only valid one being for $\lambda > 0$. Substituting the λ value, we have the projection of a 3D point $\mathbf{L}$ into parabolic surface passing by P'. The projection on the parabolic surface is defined by:

$$\mathbf{x}_p = \begin{bmatrix} x_p & y_p & \frac{R^2 - x_p^2 - y_p^2}{2R} & 1 \end{bmatrix}^T \qquad (6)$$

where

$$x_p = \frac{f_z' h f_x' - f_x' h^2 - (f_y')^2 L_x - 2 f_z' h L_x + L_x h^2 + f_y' L_y f_x' + L_z h f_x' + f_x' s_1}{ss_2}$$

$$y_p = \frac{f_z' h f_y' - f_y' h^2 - (f_x')^2 L_y - 2 f_z' h L_y + L_y h^2 + f_y' L_x f_x' + L_z h f_y' + f_x' s_1}{ss_2} \qquad (7)$$

and

$$s_1 = \sqrt{ss_0 + ss_1}$$

$$ss_0 = (|\mathbf{L}|^2 - 2p_y' L_y - 2p_x' L_x - 2p_z' L_z + |P'|^2)h^2$$

$$ss_1 = 2(p_z' p_x' L_x + p_z' p_y' L_y + p_x' L_x L_z + p_y' L_y L_z - (p_x')^2 L_z \ldots$$

$$\ldots - p_z' L_y^2 - p_z' L_x^2 - (p_y')^2 L_z)h + 2p_x' p_y' L_y L_x - (p_x')^2 L_y^2 - (p_y')^2 L_x^2$$

$$ss_2 = p_y' L_y - (p_y')^2 - (p_x')^2 - p_z' h + L_z h + p_x' L_x + s_1$$

The rays that intersect the parabolic mirror are projected to the spherical surface. This projection is in w direction, and then the relationship between the spherical surface and parabolic surface is given by:

$$R_{sp}\mathbf{x}_p + T_{sp} - \mathbf{x}_s - \lambda[0 \quad 0 \quad 1]^T = \mathbf{0}$$

where $R_{sp}x_p + T_{sp}$ is the paraboloid surface defined in the frame C. We can write x_s as:

$$\mathbf{x}_s = \begin{bmatrix} \frac{p_1}{2h} & -\frac{p_2}{2h} & \frac{4R^2h^2 - p_1^2 - p_2^2}{8h^2R} & 1 \end{bmatrix}^T \qquad (8)$$

where

$$p_1 = 2x_p h\cos\theta_y^{sp} - h^2\sin\theta_y^{sp} + x_p^2\sin\theta_y^{sp} + y_p^2\sin\theta_y^{sp} + 2t_x h$$

$$p_2 = -2y_p h\cos\theta_x^{sp} - 2t_y h - 2x_p h\sin\theta_y^{sp}\sin\theta_x^{sp} - \ldots$$

$$\ldots h^2\cos\theta_y^{sp}\sin\theta_x^{sp} + x_p^2\cos\theta_y^{sp}\sin\theta_x^{sp} + y_p^2\cos\theta_y^{sp}\sin\theta_y^{sp}$$

The x_p, y_p values are given by Equation 6. Finally, the projection into the plane image is:

$$\mathbf{u} = I_C\mathbf{x}_s \qquad (9)$$

The transformation from a real point $\mathbf{L}$ to its projected point $\mathbf{u}$ consists in:

- a change from the world, coordinate system into the parabolic coordinate system.
- the parabolic mirror reflection in direction S_z.
- the rotation and translation between the parabolic and spherical mirror.
- the perspective projection of the spherical surface to camera frame.
- finally the transformation between the camera frame and the image plane.

So, we obtain the following model:

$$u = \frac{-\alpha_u p_1}{2h}\frac{8h^2R}{4R^2h^2 - p_1^2 - p_2^2} + u_0$$

$$v = \frac{-\alpha_v p_2}{2h}\frac{8h^2R}{4R^2h^2 - p_1^2 - p_2^2} + v_0 \qquad (10)$$

where p_1, p_2 are given in Equation 8

III. CALIBRATION ALGORITHM

Given the number of parameters to estimate, it is very likely that a minimization procedure converges on a local minima if it is not properly initialized. To avoid this, our calibration algorithm uses several steps, minimizing incrementally some parameters, before refining all their estimations using Equation 10.

A first estimate of the intrinsic parameters is obtained by measuring the width of the image circle in the image, which is related to the parameter h of the parabolic mirror (see Figure 1). The spherical parameter R is twice the distance between the spherical surface and the camera lens position. These values are measured by hand in the catadioptric systems.

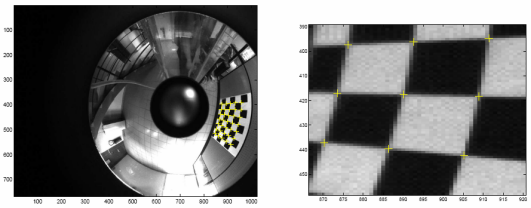

Figure 4: Calibration image example and sub-pixel corner extraction.

A. *Extrinsic parameters (R_w)*

Figure 4 shows the pattern used by the camera calibration. The patterns coordinate are known with respect to the world coordinate placed on the grid pattern. In order to compute this position with respect to the parabolic frame, one must compute the rotation and translation between the world and parabolic frames (extrinsic parameters). The intersection between the plane that contains the line V_j and the point P (in Figure 5) and parabolic mirror is given by:

$$\left(X - \frac{hp_j}{s_j}\right)^2 + \left(Y - \frac{hq_j}{s_j}\right)^2 = \frac{h^2}{s_j^2}\left(p_j^2 + q_j^2 + s_j^2\right)$$

Given points $\{(x_i, y_i)\}_{i=1}^n$ in one line of the grid (V_j or H_i), we compute the p_i, q_i, s_i values (see Figure 5) minimizing the sum:

$$f(p_j, q_j, s_j) = \sum_{i=1}^n \left(\left(X_i - \frac{h_j p_j}{s_j}\right)^2 + \left(Y_i - \frac{h_j q_j}{s_j}\right)^2 - \frac{h_j^2}{s_j^2}\left(p_j^2 + q_j^2 + s_j^2\right)\right)^2$$

by solving the equations system:

$$\frac{\partial f}{\partial p_j}=0,\frac{\partial f}{\partial q_j}=0,\ and\ \frac{\partial f}{\partial s_j}=0$$

The world frame axis W_y is given by $N(V_j)\wedge N(V_{j+1})$. We compute the W_x and W_y direction using:

$$W_y=\sum_{i=1}^{n-1}\sum_{j=i+1}^{n}\left\{N(V_i)\wedge N(V_j)\right\}$$
$$W_x=\sum_{i=1}^{n-1}\sum_{j=i+1}^{n}\left\{N(H_i)\wedge N(H_j)\right\}$$

Finally, the axis W_z is computed by $W_x\wedge W_y$. Where $\wedge$ denotes a cross product. The rotation between parabolic and world frame is computed by finding the rotation matrix that transform the w_x,w_y,w_z vectors to p_x,p_y,p_z

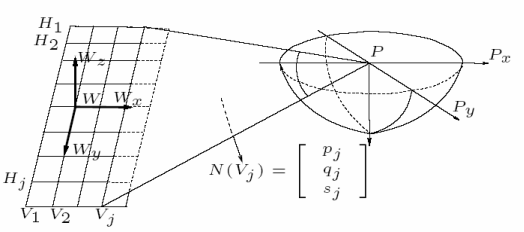

Figure 5: The line world projection into a parabolic mirror is given by the intersection between the mirror and the plane formed by the line and P.

B. Ideal camera parameters

To refine the initialization of the camera intrinsic parameters, we first consider a perfectly aligned camera model. Under this assumption, the extrinsic parameter R_w, the h and R values are recomputed as follows: the transformation of a world point L to the image point $u=(u,v)^T$ is characterized by Equation 5. The parameters of this equation are computed by minimizing

$$f(R_\omega,\mathbf{T}_\omega,\alpha_u,\alpha_v,R)=\begin{cases}\dfrac{-\alpha_u x_p(2R)}{R^2-\left(x_p^2+y_p^2\right)}+u_0-u_i\\ \dfrac{\alpha_v y_p(2R)}{R^2-\left(x_p^2+y_p^2\right)}+v_0-v_i\end{cases}\qquad(11)$$

where (u_i,v_i) are the position in pixels for the corner extracted in the images calibration (see Figure 4).

C. Fnalcalibration

The extrinsic parameters and some intrinsic parameters $(\alpha_u,\alpha_v,h,R,u_0,v_0)$ are now initialized. For the total calibration, we use Equation 10, and carry out a refinement stage by the total minimization of the following expressions:

$$F_1=\frac{-\alpha_u p_1}{2h}\frac{8h^2R}{4R^2h^2-p_1^2-p_2^2}+u_0-u_i$$
$$F_2=\frac{-\alpha_v p_2}{2h}\frac{8h^2R}{4R^2h^2-p_1^2-p_2^2}+v_0-v_i$$

where (u_i,v_i) are the pixels measured in the calibration images. The minimization uses the *Levenberg-Marquardt`s* method of Matlab, and is obtained by solving the equations system:

$$\frac{\partial F_1}{\partial\Gamma}=0\quad;\quad\frac{\partial F_2}{\partial\Gamma}=0$$

Where $\Gamma=\begin{Bmatrix}u_0,v_0,h,\alpha_u,\alpha_v,R,\theta_x,\theta_y,\\ t_x,t_y,P_x^{'},P_y^{'},P_z^{'},R_W^i,T_W^i\end{Bmatrix}$

The following table summarizes the various estimated parameters during the calibration process.

$\alpha_u,\alpha_v,u_0,v_0$	Intrinsic parameters of conventional camera
h,R	Parabolic and spherical parameters surface
$\theta_x,\theta_y,t_x,t_y,t_z$	Rotation and translation between parabolic and spherical surace
p_x',p_y',p_z'	Focal point stimation
R_wT_w	The extrinsic parameter for each image

Figure 6 shows the mean re-projection errors using the calibration parameters estimated with the ideal aligned model and with the full model, for two cameras of a stereo bench and 15 calibration frame images: the improvements are noticeable. The average re-projection errors are around 0:35 pixels, which does not seem very satisfactory with respect to conventional cameras calibration results - however, in [18] the mean re-projection error is about 0:4 pixels, and 0:5 pixels in [2] for an omnidirectional camera composed of a fish-eye lens and a conventional camera

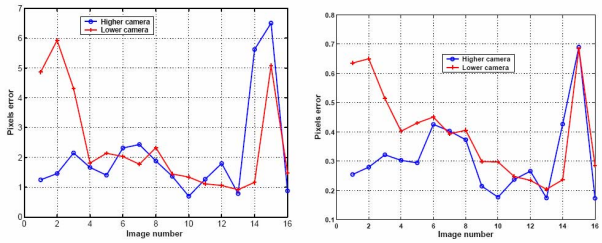

Fig. 6: Left: mean re-projection errors (in pixels) with the parameters estimated with the ideal aligned geometric model for 15 different images of the calibration frame, Right: errors obtained with the full geometric model parameters (note the scale change between the two figures).

IV. EPIPOLAR GEOMETRY ON A PARABOLIC SURFACCE

Epipolar geometry describes the relationship between the position of corresponding points in a pair of images acquired by cameras with single view-points. In this section, we consider that the panoramic images have been rectfied using the parameters of section 3 in order to obtain the ideal case of the panoramic image. Figure 7 shows the epipolar plane on catadioptric camera with parabolic mirror. The projections of the intersection of this plane and the mirror surface in the image plane are conics too. Every point q_1 onto omnidirectional image has an epipolar curve in the second mirror (l_2), represented by:

$$q_2^T A_2(E,q_1)q_2=0$$

In the generic case, the matrix $A_2(E,q_1)$ is a non linear function of the essential matrix E, the point q_1, and the calibration parameters of a central panoramic catadioptric camera.

Figure 7 shows the normal of plane Π passing by the two optical centers that can be expressed in the first mirror coordinate system:

$$\mathbf{N}_{NF1'} = \mathbf{T} \wedge \mathbf{x}_1 \quad (12)$$

The normal vector $N_{F1'}$ can be expressed in the second mirror coordinate system using E, we have:

$$\mathbf{N}_{F2'} = R\,\mathbf{N}_{F1'} = R(\mathbf{T} \wedge \mathbf{x}_1) = R[T]_x \mathbf{x}_1 = E\,\mathbf{x}_1 \quad (13)$$

where $E = \begin{bmatrix} e_{11} & e_{12} & e_{13} \\ e_{21} & e_{22} & e_{23} \\ e_{31} & e_{32} & e_{33} \end{bmatrix}$

If we set $\mathbf{N}_{F2'} = [p \quad q \quad s]^T$, we can write the equation Π in the second coordinate system:

$$pX_2 + qY_2 + sZ_2 = 0 \quad (14)$$

where $\mathbf{x}_2 = [X_2 \quad Y_2 \quad Z_2]$

Writing Z_2 as a function of X_2 and Y_2, and knowing equation of the parabolic surface, we have:

$$\left(X_2 - \frac{hp}{s}\right)^2 + \left(Y_2 - \frac{hq}{s}\right)^2 = \frac{h^2}{s^2}\left(p^2 + q^2 + s^2\right) \quad (15)$$

This is the circle equation centered in $\left(\frac{hp}{s}, \frac{hq}{s}\right)$ with radius $\frac{h}{s}\sqrt{p^2+q^2+s^2}$.

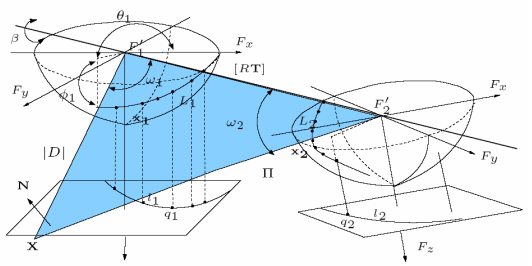

Fig. 7: Epipolar geometry between two omnidirectional cameras with parabolic mirror.

Let $\mathbf{x}_1 = [X_1 \quad Y_1 \quad Z_1]^T$ a point in the first parabolic mirror. Its epipolar curve in the second mirror is defined by L_2 (see Figure 7) and its orthographic projection on the image is represented by Equation 15, and defined by the circle l_2.

A. *Image projection criteria with the epipolar plane*

We demonstrated that l_2 is the epipolar circle in the second image for a point x_1. With the same process, we want to find the epipolar curve or curves in the first image for each point of the circle l_2.

Each point of l_2 forms with the translation vector $\mathbf{T}$ a plane which is normal to $\mathbf{N}_{F2'}$. This normal is defined in the first coordinate systems by:

$$\mathbf{N}_{F1'} = R\mathbf{N}_{F2'} = R(\mathbf{T} \wedge \mathbf{x}_2) = R[T]_x \mathbf{x}_2 = E\mathbf{x}_2 \quad (16)$$

Replacing $\mathbf{N}_{F2'}$ of Equation 13 in Equation 14, we have

$$e_{11}X_1X_2 + e_{12}Y_1X_2 + e_{13}Z_1X_2 + e_{21}X_1Y_2 + \ldots$$
$$e_{22}Y_1Y_2 + e_{23}Z_1Y_2 + e_{31}X_1Z_2 + e_{32}Y_1Z_2 + e_{33}Z_1Z_2 = 0$$

where $Z_1 = \frac{h^2 - X_1^2 - Y_1^2}{2h}$

We can write the last equation in the following form:

$$\left(X_1 - \frac{hP}{S}\right)^2 + \left(Y_1 - \frac{hQ}{S}\right)^2 = \frac{h^2}{S^2}\left(P^2 + Q^2 + S^2\right) \quad (17)$$

where $\begin{bmatrix} P \\ Q \\ S \end{bmatrix} = \begin{bmatrix} e_{11} & e_{21} & e_{31} \\ e_{12} & e_{22} & e_{32} \\ e_{13} & e_{23} & e_{33} \end{bmatrix} \begin{bmatrix} X_2 \\ Y_2 \\ Z_2 \end{bmatrix}$

The vector $[P \quad Q \quad S]^T$ is defined by Equation 16. The epipolar curve of the circle l_2 is defined by Equation 17 and is a circle too.

In two panoramic catadioptric cameras with a translation and rotation between them, we have a set of circles l_1 and l_2, where l_2 is the epipolar circle of l_1 and vice versa (see Figure 7). These circles are the perpendicular projections of the intersection between the two parabolic mirrors with a plane that contains the centers of the parabolic mirrors. The l_1 and l_2 equations are functions of the essential matrix E (Equations 15 and 17).

We use this property in order to generate rectified images, in which epipolar lines are parallel. The algorithm is as follows:

- Given a translation and rotation $[\mathbf{T}, R]$ between two cameras,

$\Pi_1^\tau = \{P_1 \in \Re \mid < P_1F_1, \mathbf{T} >= 0\}$

$\Pi_2^\tau = \{P_2 \in \Re \mid < P_2F_2, R\mathbf{T} >= 0\}$

- We choose a point $P_1^1 = \{P_1^1 \in \Pi_1^\tau\}$
- Initalize $\beta^i \leftarrow 0$ and $P_1^i \leftarrow P_1^1$
- **do**
  - The epipolar plane of P_1^i

  $\Pi_1^\beta = \{Q_1 \in \Re \mid < Q_1, Q_1^iF_1, \mathbf{T} >= 0, Q_1^i \in \Pi_1^\tau\}$

  $\Pi_2^\beta = \{Q_2 \in \Re \mid < Q_2, Q_2^iF_2, R\mathbf{T} >= 0\}$
  - Initialize

  $Q_1^i \leftarrow P_1^i$

  $Q_2^i \leftarrow \{Q_2^i \in \Re \mid Q_2^i \in \Pi_2^\tau, Q_2^i \in \Pi_2^\beta\}$

  $\alpha^i \leftarrow 0$
- **do**

  omnidirectional image sampling

  $x_1^i(\beta,\alpha) = I_C\,\Im(Q_1^i)$ (Equation 5)

  $x_2^i(\beta,\alpha) = I_C\,\Im(Q_2^i)$ (Equation 5)

  $Q_1^{i+1} = \wp(Q_1^i, \alpha_i, Q_1^iF_1 \wedge \mathbf{T})$

  $Q_2^{i+1} = \wp(Q_2^i, \alpha_i, \overline{Q_2^iF_2} \wedge R\mathbf{T})$

  $\alpha^{i+1} = \alpha^i + \Delta\alpha$
  - **while** ($\alpha^{i+1} \le 2\pi$)

  $P_1^{i+1} = \wp(P_1^i, \beta^i, \mathbf{T})$

  $\beta^{i+1} = \beta^i + \Delta\beta$
- **while** ($\beta^{i+1} \le 2\pi$)

Warping algorithm. The subscript $1,2,k = 1,2$ define the reference frame, while the superscript i is the iteration number. The rotation function $\wp(A,B,C)$ turn the point A,B degrees around of the axis C. These rotations are computed with Rodriguez equation. The function $\Im(Q_k^i)$ projected the point Q^i (defined in the to parabolic frame k) to the parabolic surface k in direction Q_kF_k. The warping image is defined by $x_{1,2}^i(\beta,\alpha)$

B. 3D reconstruction

If we know the rotation (R), translation ($\mathbf{T}$) between two cameras and the intrinsic parameters, we can compute the tables that allows us to rectify the panoramic images. In this process, we can also compute the tables that contain the angular values $(\theta_1, \phi_1, \varpi_1, \varpi_2)$ for each rectified pixel (see Figure 7). These angles are defined by:

$$\theta_1 = \arctan\left(\frac{y_1}{x_1}\right) \qquad \phi = \arcsin\left(\frac{z_1}{\sqrt{x_1^2 + y_1^2}}\right) \qquad (18)$$

$$\omega_1 = \arccos\left(\frac{\mathbf{x}_1^T \mathbf{T}}{|\mathbf{x}_1||\mathbf{T}|}\right) \quad \omega_2 = \arccos\left(\frac{\mathbf{x}_2^T R\mathbf{T}}{|\mathbf{x}_2||R\mathbf{T}|}\right)$$

Where x_1 and x_2 are the projections of a point 3D to parabolic surface 1 and 2.

Knowing the coordinates of two matched points x_1 and x_2 that correspond to the same 3D point $\mathbf{X}$, we can compute the coordinate of $\mathbf{X}$ in the frame F_1:

$$\mathbf{X} = \left[|D|\sin\theta_1 \quad |D|\cos\theta_1 \quad |D|\sin\phi_1\right]^T \qquad (19)$$

where $|D| = \dfrac{\sin\omega_2}{|\mathbf{T}|\sin(\omega_1 + \omega_2)}$

Figure 8 shows the warped images and 3D reconstruction for the real panoramic images acquired with the cameras calibrated in section 3.

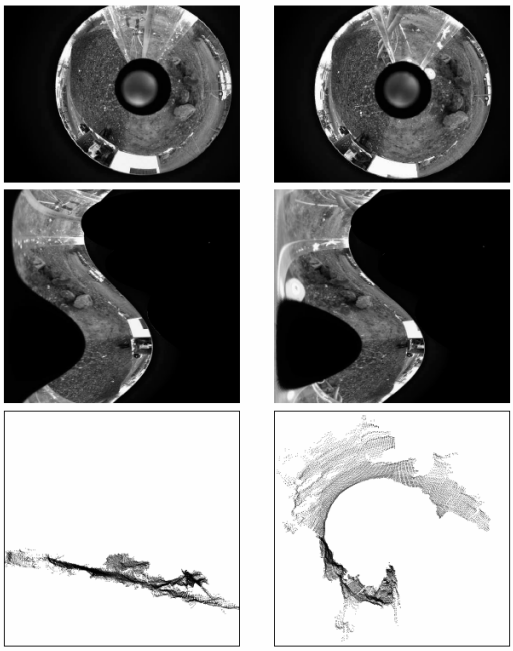

Fig. 8: Stereovision result. From top to bottom: original images acquired with the two cameras, rectified images, and two views of the 3D reconstruction. Note the "blind area", due to the mast that supports the cameras.

V. SUMMARY

We presented a complete characterization of a catadioptric camera with parabolic and spherical mirrors, which takes into account the alignment errors between the mirrors. In such a configuration, the projection of the parabolic mirror is not orthogonal, and the incidental rays therefore do not cross the focus of the paraboloid. To cope with this, we introduced a model in which the single viewpoint does not perfectly match the paraboloid focus. We used this characterization to calibrate for camera calibration in several steps, which enables to ensure the convergence of the estimate of the parameters of the model.

We presented the equations of the epipolar curves in panoramic images, and introduced a rectifying method that transform the epipolar curves into parallel straight lines. This makes possible to carry out a dense pixel matching algorithm with good computing time performance. The method is independent of the configuration of the stereo bench.

REFERENCES

[1] J. Baldwin and A. Basu. 3d estimation using panoramic stereo. In International Conference on Pattern Recognition, pages 91-100, 2000.

[2] Hynek Bankstein and Tomas Pajdla. Panoramic mosaicing with a 180 field of view lens. IEEE Workshop on Omnidi- rectional Vision, June 2002.

[3] Basu and J. Baldwin. A real-time panoramic stereo imaging system and its application. Springer, 2001.

[4] Roland Bunshoten and Ben Krse. Range estimation from a pair of omnidirectional images. In International Conference on Robotics and Automation, pages 1174-1179, May 21-26 2001.

[5] Cyril CAUCHOIS, Eric BRASSART, Cyril DROCOURT, and Pascal VASSEUR. Calibration of the omnidirectional vision sensor : Syclop. In Proc. of the IEEE International Conference on Robotics and Automation, pages 1287 -1292, May 1999.

[6] J. Fabrizio, J.-P. Tarel, and R. Benosman. Calibration of panoramic catadioptric sensors made easier. In n IEEE Workshop on Omnidirectional Vision (Omnivis'02), June 2002.

[7] Olivier Faugeras. Three-Dimensional Computer Vision a Geometric Viewpoint. The MIT Press Cambridge, Massachusetts, Juin 1993.

[8] Christopher Geyer and Kostas Daniilidis. Catadioptric camera calibration. International Conference in Computer Vision, 1999.

[9] Joshua Gluckman, Shree K. Nayar, and Keith J. Thoresz. Real-time omnidirectional and panoramic stereo. In Image Understanding Workshop, 1998.

[10] S. B. Kang and R Szeliski. 3-d scene data recovery using omnidirectional multibaseline stereo. International Journal of Computer Vision, 25(2):167-183, November 1997.

[11] Sing Bing Kang. Catadioptric self-calibration. In Computer Vision and Pattern Recognition, 2000.

[12] Hiroshi Koyasu, Jun Miura, and Yoshiaki Shirai. Racognizing moving obstacles for robot navigation using real-time omnidirectional stereo vision. Journal of Roboics and Mechatronics, 14(2):147-156, 2002.

[13] Branislav Micusik. Two-View Geometry of Omnidirectional Cameras. PhD thesis, Czech Technical University, Karlovo namesti 13, 12135 Prague Prague 2, Czch Republic, June 2004.

[14] Shree K. Nayar. Catadioptric omnidirectional camera. In Computer Vision and Pattern Recognition, 1997.

[15] Shree K. Nayar. Omnidirectional vision. The Eighth International Symposium of Robotics Research, October 1997.

[16] Kim C. Ng, Mohan Trivedi, and Hiroshi Ishiguro. Generalize multiple baseline stereo and direct virtual view synthesis using range-space search, match, and render. International Journal of Computer Vision, 47(1/2/3):131-147, April-June 2002.

[17] T. Sogo. Real-time target localization and tracking by n-ocular stereo. In Proceedings of the IEEE Workshop on Omnidirectional Vision, pages 153-160, 2000.

[18] Dennis Strelow, Je_rey Mishler, David Koes, and Sanjiv Singh. Precise omnidirectional camera calibration. In Computer Vision and Pattern Recognition, 2001.

[19] Changming Sun and Shmuel Peleg. Fast panoramic stereo matching using cylindrical maximum surfaces. Transactions on Systems, man, and Cybermetics Part B: Cybermetics, 34:760-765, Feb 2004.

[20] Jun Takiguchi, Minoru Yoshida, Akito Takeya, Jyin ichi Eino, and Takumi Hashizume. High precision range estimation from an omnidirectional stereo system. In Int. Conference on Intelligent Robots and Systems, pages 263-268, October 2002.